Estimating Above-ground Biomass of Trees Outside Forests in the Thar Desert using Sentinel Data and Machine Learning

Kapil Kumar[1], A.S. Anjitha[2], Dhruv Swami[1], Sandeep Kumar[1], C. Sudhakar Reddy[3]*
[1]Department of Botany, Government Lohia College, Churu, Rajasthan, India
[2]Department of Environmental Sciences, All Saints' College, Affiliated to University of Kerala, Thiruvananthapuram, Kerala, India
[3]Forest Biodiversity and Ecology Division, National Remote Sensing Centre, Indian Space Research Organisation, Balanagar, Hyderabad, Telangana, India
*Corresponding Author email: drsudhakarreddy@gmail.com

(Received on 15 August 2025; In final form on 13 April 2026)

DOI: *https://doi.org/10.58825/jog.2026.20.1.281*

Abstract: Above-ground biomass estimation of Trees outside Forests is crucial as they play a significant role in carbon sequestration, biodiversity conservation, and microclimate regulation, especially in arid and semi-arid regions where tree cover is limited. The heterogeneous vegetation covers and highly scattered nature of trees add to the challenges in the accurate estimation of aboveground biomass employing remote sensing technology. This study aimed to estimate the AGB of TOF in the arid regional landscape of the Thar desert of Rajasthan, integrating Sentinel-1 (S1) SAR and Sentinel-2 (S2) optical datasets and field observations, applying the Random Forest (RF) model. The field calculated AGB in the sampled area ranged from a minimum of 0.19 t/ha to a maximum of 43.12 t/ha, with a mean of 8.03 t/ha. The backscattering coefficients at VV and VH polarizations and 5 SAR indices from S1 and the multispectral bands, vegetation indices, and biophysical variables from S2 were extracted as the predictor variables for the AGB model. After correlation and multi-collinearity analysis, three models were developed: the first model based on S1(M_S1), the second model with S2 (M_S2), and the third model is a combined model of S1 and S2 variables (M_S1S2). The correlation analysis revealed that the SAR indices have a higher relationship with field biomass. Further, the combined model (M_S1S2) achieved the highest accuracy (R^2 = 0.52, RMSE = 3.89 t/ha) in AGB estimation, followed by M_S1 (R^2 = 0.46) and M_S2 (R^2 = 0.43). The results of the study highlight the utility of Sentinel datasets and larger ecological plots at the landscape level in biomass mapping in sparsely vegetated arid environments. Moreover, the study highlights the ecological importance of TOF and emphasizes the need for biomass and carbon stock assessments in the ecologically sensitive arid regions.

Keywords: Aboveground biomass, Trees, Remote sensing, SAR, Multispectral, Machine learning

1. Introduction

The term "trees outside forests" (TOF) was included in the context of global forest monitoring during the planning phase of the Global Forest Resources Assessment (FRA) 2000, an initiative by the Food and Agriculture Organization (FAO) of the United Nations (Schnell et al. 2014). As a crucial natural resource, TOF- including trees along roadsides, railways, canals, within settlements, and in agroforestry systems- plays a significant role in contributing to biomass at regional and national levels. Additionally, it supports the sustainable management of resources by providing diverse goods and services that benefit both people and ecosystems (Anjitha et al. 2024). In arid and semi-arid environments, where natural forest cover is limited, TOF plays a major role in sequestering atmospheric carbon dioxide through photosynthesis and accumulating it as biomass (FAO 2005; Singh and Chand, 2012). Above-ground biomass is considered an essential climate variable and a potential biodiversity variable for understanding changes in the climate–vegetation system and ecosystem function (Reddy et al. 2025).

Estimating the carbon sequestration potential of TOF helps to understand the terrestrial carbon dynamics more completely. The carbon sequestration potential of vegetation is directly linked to its biomass, as greater biomass results in higher carbon stock, which serves as a key indicator of the ability of plants to capture and store atmospheric carbon over time. Remote sensing (RS) technology offers a fast, cost-effective, and reliable approach in estimating the vegetation biomass and carbon stock over large areas (Bordoloi et al. 2022; Sainuddin et al. 2023; Sulabha et al. 2025). However, ground truth measurements are indispensable for calibration and validation of the models (Adam et al. 2009; Imran et al. 2020). Researchers have explored the potential of several RS datasets in estimating AGB of vegetation, including optical, radar, hyperspectral, and LiDAR (Santos et al. 2009; Kumar and Mutanga, 2017; Kumar et al. 2012; Kumar et al. 2019; Hu et al. 2016; Sun et al. 2019; Van Pham et al. 2019; Carreiras et al. 2012; Anand et al. 2020; Pandey et al. 2019; Srivastava et al. 2020). Multispectral bands, vegetation indices, biophysical variables, texture features, backscattering coefficients, and canopy height are the major variables extracted from RS datasets in biomass estimation studies.

Researchers have derived multiple vegetation indices from the remote sensing datasets and found a considerable relationship with biomass. AGB in the Mangrove forest in the Zambales province was estimated by (Baloloy et al. 2018) with a higher prediction accuracy of 0.92 for the S2-based Multivariate Adaptive Regression Spline model.

The microwave (Sentinel-1) and optical (Sentinel-2) data of the European Space Agency have been used for vegetation biomass estimation singularly or complementarily at different ecoregions (Chang et al. 2016; Castillo et al. 2017; Agata et al. 2018; Torabzadeh et al. 2019; Malhi et al. 2022; Cartus et al. 2022; Nuthamachot et al. 2020; Forkuor et al. 2020; Rapiya et al. 2023). AGB in the Shoolpaneshwar Wildlife Sanctuary (SWS), Gujarat, India, was estimated by (Malhi et al. 2022), and it was observed that combining backscattering coefficients and vegetation indices can improve the prediction. (Nuthamachot et al. 2020) combined S1 and S2 variables for improving the biomass estimation in the private forest of Yogyakarta Province, Indonesia, and obtained a higher R^2 value of 0.84. (David et al. 2022) estimated the dryland forest biomass by combining S1 backscatter and S2 vegetation indices. The AGB prediction Extreme Gradient Boosting (XGB) model based on S1 and S2 variables gave an R^2 of 0.61 and RMSE of 37.85 t/ha in the Purna wildlife sanctuary.

Although Trees Outside Forests (TOF) play a vital role in carbon accounting and climate change mitigation, they have received considerably less scientific attention compared to the estimation of biomass and carbon stocks in forested areas. A limited number of studies have focused on AGB estimation of TOF. (Anjitha et al. 2024) estimated the above-ground biomass of TOF in the semi-arid region of Sri Sathya Sai district of Andhra Pradesh, India, using ALOS PALSAR-2 and Sentinel-1 datasets with an RF model, getting an R^2 value of 0.64.

Estimating the AGB of vegetation is vital, especially in the arid and semi-arid regions where TOF makes the dominant perennial vegetation, continually sequestering the atmospheric carbon dioxide over long periods. However, field sampling faces difficulties mainly stemming from the heterogeneous and highly scattered nature of the trees across mixed land use mosaics. This necessitates the establishment of large-scale ecological plots to capture and understand the true distribution and variability in the vegetation biomass. Furthermore, although RS technology is advantageous for vegetation biomass mapping, in arid and semi-arid regions, it is associated with numerous challenges that are not typically encountered in humid and sub-humid areas. The primary obstacles include low vegetation signal-to-noise ratio, strong background reflectance from the soil, highly variable spatial distribution of vegetation, and unreliable growing seasons (Bestelmeyer et al. 2015; Cheng et al. 2017; Haughton et al. 2018; Issa et al. 2020). The weak spectral signal from the sparse vegetation is often lost within the satellite pixel or obscured by the background. Incorporation of multi-sensor datasets and vegetation indices can overcome these limitations. For instance, variations of soil-adjusted VIs such as soil adjusted vegetation index (SAVI), and transformed SAVI (TSAVI), modified SAVI (MSAVI) were used by (Zandler et al. 2015) to compensate the soil brightness in mapping total biomass of sparse vegetation cover. In this study, we estimated the AGB of TOF in the arid region of Rajasthan, India, with scattered trees, utilizing the field inventory from large-area ecological plots and remote sensing datasets from Sentinel-1 and Sentinel-2 missions and the random forest regression model. In addition, we evaluated the capability of these datasets individually and in synergy in estimating the AGB of TOF.

2. Study Area

The study area selected for this study is the arid region spanning three districts, such as Churu, Sikar, and Jhunjhunun, Rajasthan, India, where the majority of the area falls in the Churu district (Figure 1). This arid regional landscape, taken for the study, covers an area of 625 km^2. It is known as the gateway of the Great Indian (Thar) Desert. It experiences a typical hot desert climate, with summer temperatures soaring above 45°C and winter temperatures dropping to 5°C. Annual rainfalls is highly erratic, averaging 200–300 mm, during the monsoon season (July–September), with frequent droughts exacerbating water scarcity (Kar et al. 2009). It lies in the Hyper Arid Partial Irrigated Western Plains Agro-Climatic Zone (https://foundation.rajasthan.gov.in/rf/pdf/Churu.pdf).

3. Methodology

3.1 Field Data

An area of 1,089 ha was chosen within the regional landscape for achieving a better understanding of tree distribution, and utilizing high-resolution Google Earth imagery (Google), every individual tree was geolocated and mapped. Further, the sampling area was divided into 100 × 100 m grid cells (equivalent to 1 hectare) to analyse the spatial distribution pattern of trees in rural and urban landscapes. Field sampling was carried out during December 2024 and January 2025 across four land use/land cover types, comprising one large plot in an urban landscape (20 ha) and four plots in rural landscape, including cropland (10 ha), scrubland (5 ha), and rural settlement (10 ha). Subsequently, ~ 0.1 ha grid was laid on the sampling area, and tree information from the pixels was extracted. The subplots having a minimum of three trees were selected for further analysis and estimation of AGB, which comprised a total of 132 plots, making this sampled area equivalent to 0.064% of the total area selected. A global positioning system (GPS) was used to record the geographical coordinates of the sampling plots, and the height and diameter at breast height of individual trees, and species names were noted to calculate AGB using an allometric equation (Chave et al. 2014). Despite several allometric equations having been developed for different plant species, only a few are available for the plant species in the desert and arid regions (Issa et al. 2020). Moreover, multispecies allometric models offer greater methodological efficiency for biomass estimation. We adopted this generalized pantropical equation, which includes the easily measurable variables, including the height, DBH, and wood density, instead of species-specific allometric equations, as this could possibly reduce the compounding errors from multiple species-specific models.

$$AGB = 0.0673 * (\rho * D2 * H)0.976 \quad \text{Eq. 1.}$$

where ρ - specific wood density in g/cm^3,
D - diameter at breast height (DBH) in cm
H - height in m

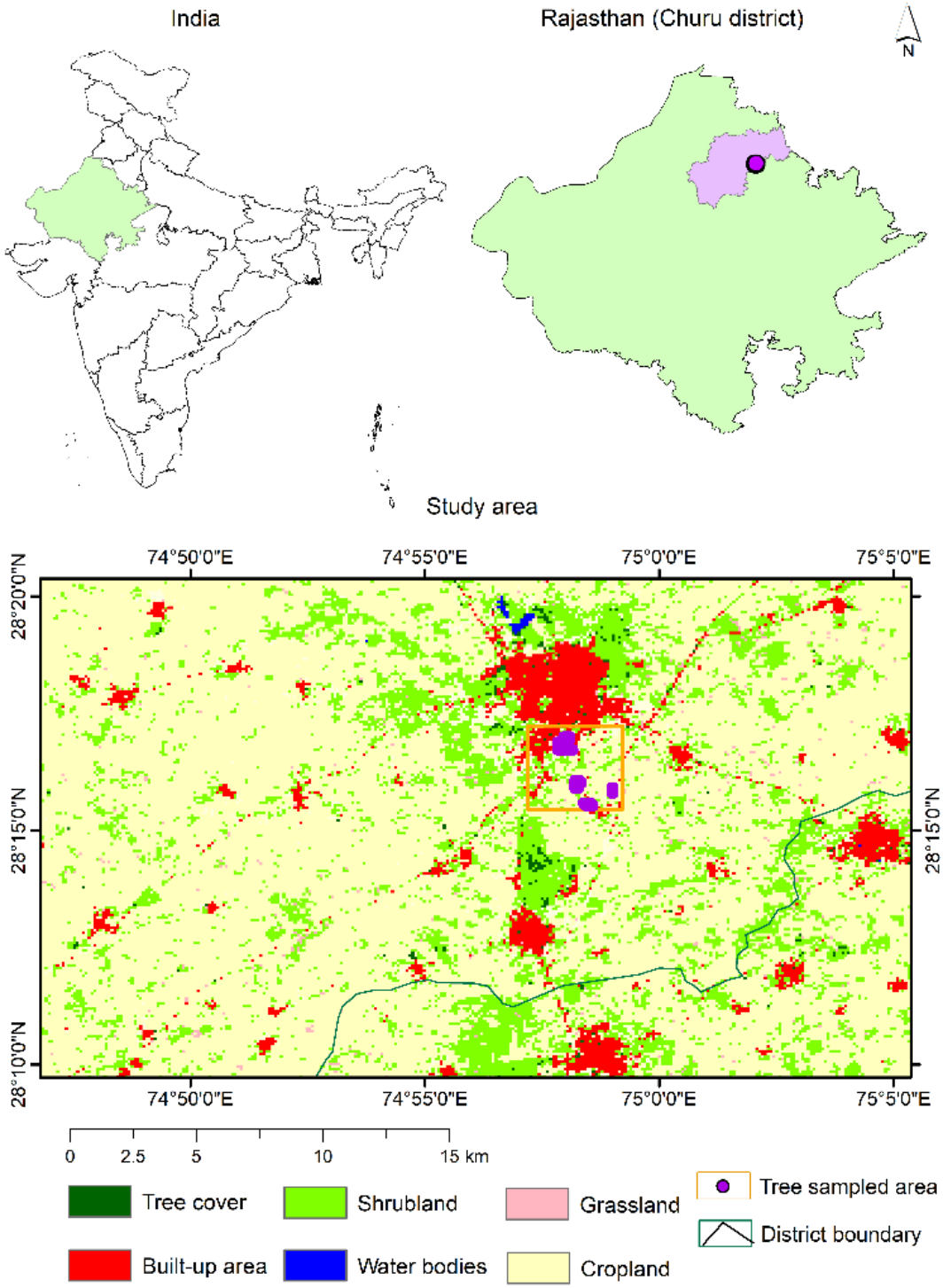

Figure 1: Study Area Map Showing Classified Vegetation Types and Land Cover (ESA, 2020)

3.2 Remote Sensing Data and Predictor Variables

The remote sensing datasets used in this study are from the Sentinel-1 (S1) and Sentinel-2 (S2) missions of the European Space Agency, which provide valuable Earth observation datasets for environmental monitoring. S1 is equipped with a C-band SAR, providing all-weather, day and night imaging capabilities. S2 is equipped with a multispectral optical sensor, which captures high-resolution imagery in 13 spectral bands. Both these datasets were freely accessed from the ESA's Copernicus Data Space Ecosystem browser (https://dataspace.copernicus.eu/).

The SAR data from the S1 mission was obtained in the Ground Range Detected (GRD) format with the date of acquisition 23rd January 2025, in the IW mode. The GRD data are multilooked and ground range detected using an Earth ellipsoid model and are composed of square pixels (Filipponi, 2019). This dual-polarized (VV+VH), high-resolution dataset was pre-processed in SNAP software. A detailed description of S1 and S2 is given in Table 1. The RS datasets were acquired for the dates that closely align with the field sampling period, as the vegetation dynamics are expected to be minimal in the short temporal window. Hence single dataset from SAR and optical sensors has been selected as representative of the field conditions.

Table 1: Data Description of Remote Sensing Datasets Used in the Study

Parameter	Sentinel-1	Sentinel-2
Mission Type	Radar Imaging	Optical Imaging
Sensor Type	C-band SAR	Multispectral Instrument (MSI)
Operating Frequency/Bands	C-band (5.405 GHz)	13 spectral bands (from visible to SWIR)
Polarization Mode	Dual (VV+VH)	Not applicable
Data Acquisition Mode	Interferometric Wide (IW)	Multispectral imaging
Spatial Resolution	10 m × 10 m	10m, 20m, 60m
Temporal resolution (Revisit Time)	6 days	5 days
Swath Width	250 km	290 km
Date of Acquisition	23/01/2025	26/01/2025

The pre-processing steps involved in Sentinel-1 data processing are illustrated in Figure 2. The first step involved applying the orbit file, which provides the precise position of the satellites and information regarding the velocity, as the orbit state vectors within the metadata of SAR products are usually not reliable. The additive thermal noise was then removed, normalizing the backscatter signals, which otherwise would disturb the intensity of the image. Further, the low-intensity noise and invalid data on the edges of the scenes were removed through border noise removal. The next step involved in the preprocessing was to convert the DN values of each pixel to the radiometrically calibrated backscattering coefficients (σ0).

The Refined Lee filter was employed to reduce the speckles in the data. Speckles in the images are salt and pepper-like granular noise, occurring with the interference of waves that have reflected back from various elementary scatterers (Lee et al. 1994). Speckle filtering helps in enhancing the quality of the images. Moreover, Range Doppler terrain correction was performed using the SRTM 1 arc second DEM to compensate for the distortions such as foreshortening, layover, and shadows, related to the side-looking geometry of the radar system. This enables the geometric representation of the images to be as close to the real world as possible (Small and Schubert, 2008; Filipponi, 2019). Finally, the backscattering coefficients (σ0) were converted to decibel units using Eq.2. In addition to the backscattering coefficients, 5 SAR indices were calculated from the backscatter images in decibel units as well, including the SAR additive index (SAI), SAR difference index (SDI), SAR multiplicative index (SMI), SAR simple ratio index (SSRI), and SAR vegetation index (SRVI).

$$\Sigma 0\ (db) = 10\log 10\sigma 0 \qquad \text{Eq. 2.}$$

S2 multispectral datasets provide data at three resolutions: 10, 20, and 60m. We acquired the Level 2A data with the date of acquisition 26th January 2025. The variables taken from S2 include the bands, vegetation indices, and biophysical variables. The VIs were calculated using the terra package in R software. Nine VIs were calculated, including normalized difference vegetation index (NDVI), Green NDVI (GNDVI), Enhanced vegetation index (EVI), Enhanced vegetation index (EVI2), ratio vegetation index (RVI), normalized difference infrared index (NDII), normalized difference red-edge index (NDRE), soil adjusted vegetation index (SAVI), and red-edge chlorophyll index (RECl).

In addition, five biophysical variables (BPVs) were extracted from S2 using SNAP software. They are strongly associated with the vegetation health, structure, productivity, condition, and dynamics, hence will have a significant influence in biomass estimation (Baloloy et al. 2018). The BPVs used are leaf chlorophyll content (CAB), canopy water content (CWC), fractional vegetation cover (FCOVER), fraction of absorbed photosynthetically active radiation (FAPAR), and leaf area index (LAI). Table 2. gives the RS variables used in the study.

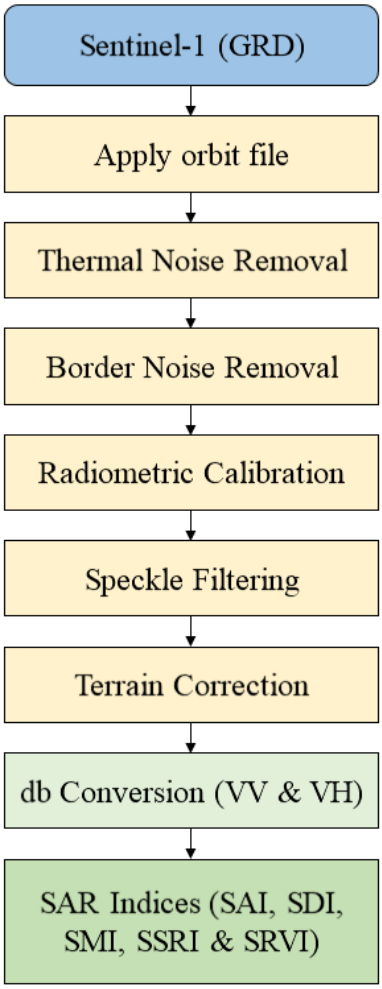

Figure 2: Workflow of Sentinel-1 SAR Data Processing

Table 2: RS-based Predictor Variables Extracted for AGB Estimation

Sensor	Predictor variable		Definition	Reference
S1 (GRD data)	Backscattering coefficients	VH	Vertical transmit and horizontal received channel	
		VV	Vertical transmit and vertical received channel	_____
	Polarization indices	SAI	VH + VV	
		SDI	VH - VV	
		SMI	VH * VV	_____
		SSRI	VH/VV	
		SRVI	4σ0VH/ (σ0VV + σ0VH)	Nasirzadehdizaji et al. 2019
S2 (Level 2A)	Bands	B2	Blue, 490 nm	
		B3	Green, 560 nm	
		B4	Red, 665 nm	
		B5	Red edge, 705 nm	_____
		B6	Red edge, 749 nm	

		B7	Red edge, 783 nm	
		B8	Near Infrared, 842 nm	
		B9	Near Infrared, 945nm	
		B10	Short Wave IR, 1375 nm	
		B11	Short Wave IR, 1610 nm	
		B12	Short Wave IR, 2190 nm	
	Vegetation Indices	NDVI	(NIR-R) / (NIR+R)	Rouse et al. 1974
		GNDVI	(NIR-G) / (NIR+G)	Gitelson et al. 1996
		EVI	2.5 * ((NIR-R)/(NIR+6*R-7.5*B+1))	Liu et al. 1995
		EVI2	2.5 * ((NIR - R) / (NIR + 2.4 * R + 1)	Jiang et al. 2008
		NDII	((NIR-R) / (NIR+R+L))*(1+L)	Hunt et al. 1989
		SAVI	(1 + 0.5) * (NIR-R) / (NIR+R+0.5)	Huete, 1988
		RECl	NIR/Red Edge - 1	Gitelson, 2005
		RVI	NIR/R	Jordan, 1969
		NDRE	(NIR-Red Edge) / (NIR+Red Edge)	Gitelson et al. 1994
	Biophysical Variables	CAB	Leaf chlorophyll content	_____
		CWC	Canopy water content	
		FCOVER	Fractional vegetation cover	
		FAPAR	Fraction of absorbed photo-synthetically active radiation	
		LAI	Leaf area index	

3.3 Correlation and Multi-collinearity Analysis

To assess the strength and direction of relationships among the predictor variables and with the dependent variable, Pearson correlation analysis was carried out. Further, multicollinearity analysis was performed to identify and remove the interdependent variables, as they may carry overlapping information that could influence the stability of the regression model.

3.4 AGB Model Building and Validation

We used a random forest (RF) machine learning algorithm (MLA) for AGB modelling in this study. RF is an ensemble MLA used for both regression and classification. It was developed by (Leo Breiman 2001). This algorithm is chosen for its predictive accuracy, capability to handle high-dimensional data effectively, and robustness to noise and outliers. To analyze the potential of S1 and S2 datasets, three models were developed by incorporating the variables from individual sensors (M_S1 and M_S2) and combining the variables from both sensors (M_S1S2). The whole dataset was divided into training (80%) and testing (20%) datasets. The training dataset was used to develop the models, and the testing dataset was used for validation of the developed models. Model validation is an important step in evaluating the robustness and applicability of the developed approach. Three metrics, coefficient of determination (R^2), root mean square error (RMSE), and mean absolute error (MAE), were used in validation. Based on the metrics, the models were compared for performance, and the spatial map for AGB for the study area was created in ArcMap 10.8. To extract the vegetation class of the study area, we masked the non-vegetated area using NDVI. The overall methodology adopted for the study is depicted in Figure 3.

$$R^2 = 1 - \frac{\sum_{i=1}^{n}(y_i - \hat{y}_i)^2}{\sum_{i=1}^{n}(y_i - \bar{y}_i)^2} \quad \text{Eq. 3}$$

$$\text{RMSE} = \sqrt{\sum_{i=1}^{n} \frac{(\hat{y}_i - y_i)^2}{N}} \quad \text{Eq. 4}$$

$$\text{MAE} = \frac{1}{N}\sum_{i=1}^{n}|\hat{y}_i - y_i| \quad \text{Eq. 5}$$

where, y_i - observed AGB,
$\hat{y}_i$ - predicted AGB,
$\bar{y}_i$ - mean of observed AGB, and
N - number of data used for evaluation.

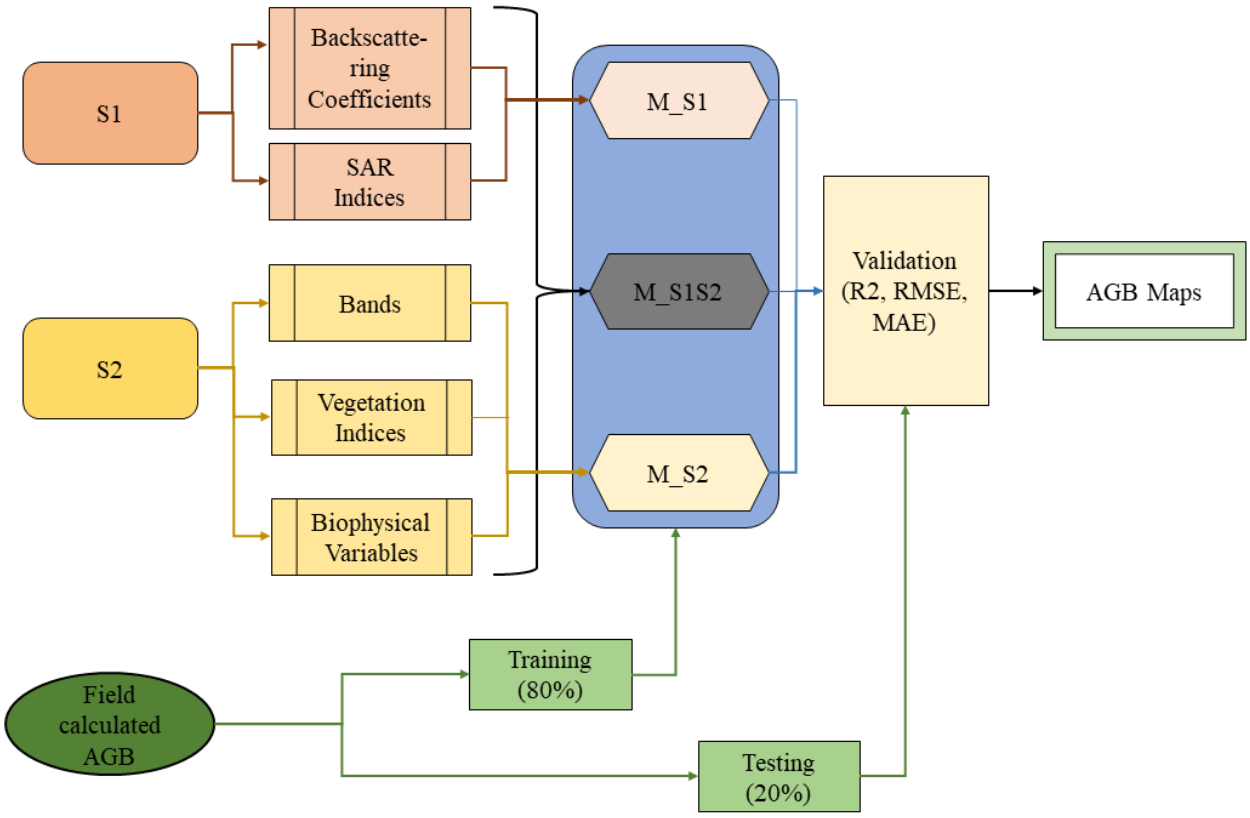

Figure 3: Flowchart Depicting the Methodological Framework Used for AGB Estimation

4. Results and Discussion

4.1 Tree Density and Composition

In the mapped area of 1,089 hectares, tree density ranged from 1 to 98 trees per hectare, with a mean of 21.4 trees/ha, a median of 19 trees/ha, and a standard deviation of 12.6 trees/ha (Figure 4, 5). This variation reflects the heterogeneity of tree distribution across different land cover types (Figure 6). Of the 41 tree species sampled, *Prosopis cineraria* is dominant with 27% of individuals followed by *Azadirachta indica, Dalbergia sissoo, Ziziphus mauritiana, Tecomella undulata, Polyalthia longifolia, Syzygium cumini, Acacia tortilis, Acacia nilotica, Albizia lebbeck, Phyllanthus emblica, Ailanthus excelsa, Moringa oleifera, Tecoma stans, Capparis decidua,* and *Prosopis juliflora.* The major tree species highly contributing to the density in rural areas were observed to vary across the rural and urban landscapes due to differences in land use and land cover. In rural areas, native and drought-resistant species such as *Ailanthus excelsa, Azadirachta indica, Prosopis cineraria, Prosopis juliflora, Dalbergia sissoo, Tecomella undulata,* and *Ziziphus mauritiana* were dominant. These species are well adapted to the arid conditions and are found along the cropland and scrub lands of the rural landscape. Compared to rural landscape, urban area was more diverse in tree species, including native and ornamental species other than the trees found in rural areas, such as *Acacia tortilis, Aegle marmelos, Albizia lebbeck, Alstonia scholaris, Conocarpus erectus, Polyalthia longifolia, Psidium guajava, Syzygium cumini, Tamarindus indica,* and *Tecoma stans.*

Further, among the 132 field plots, 63 were in the urban landscape and 69 were in the rural landscape, of which 28 were in the cropland and 8 were in the scrubland. The number of trees in each plot ranged from 3 to 8, suggesting that the plots had a sparse vegetation cover. Table 3. indicates the distribution of 132 sample plots based on number of trees per plot in urban and rural landscapes.

4.2 Field Biomass

Field-calculated AGB among the 132 sampling plots ranged from 0.19 t/ha to 43.12 t/ha with a mean of 8.03 t/ha and a standard deviation (SD) of 7.04 t/ha. Figure 7. shows the boxplot of field-calculated AGB. The field observed AGB in the rural landscape and the urban landscape was in the range of 1.06 t/ha to 25.22 t/ha and 0.19 t/ha and 43.12 t/ha, respectively. A statistical summary of the field AGB is given in Table 4. Moreover, the highest aggregated contribution of AGB (>5 t/ha) in the sampled area was from 4 tree species, such as *Ficus religiosa* (5.1 t/ha), *Dalbergia sissoo* (10.13 t/ha), *Azadirachta indica* (18.63 t/ha) and *Prosopis cineraria* (54.95 t/ha). In contrast, *Manilkara zapota* (0.006 t/ha), *Acasia catechu* (0.012 t/ha), *Plumeria obtuse* (0.015 t/ha), *Citrus limon* (0.028 t/ha), *Elaeocarpus ganitrus* (0.037 t/ha), *Nerium indicum* (0.039 t/ha), *Ficus benghalensis* (0.047 t/ha) and *Morus alba* (0.047 t/ha) were the least contributing tree species in aggregate species wise AGB (<0.05 t/ha). Further, to prevent the misleading predictions and to enhance the model performance, the outliers in the whole data, irrespective of urban and rural, were removed, resulting in 123 plots, where the maximum and mean AGB observed were 17.95 t/ha and 6.64 t/ha, respectively.

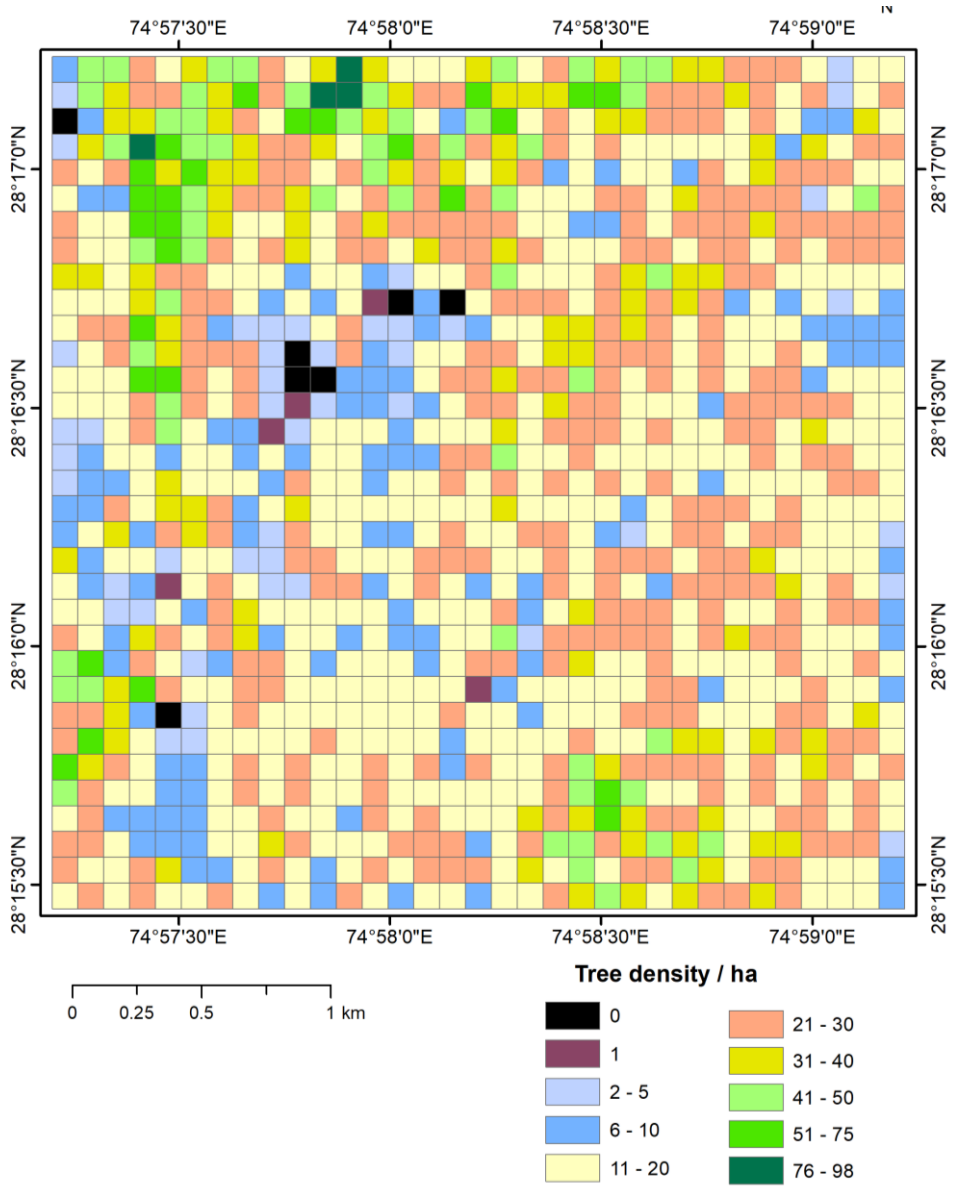

Figure 4: Spatial Distribution of Trees in the Tree-sampled Area of the Churu District, Rajasthan

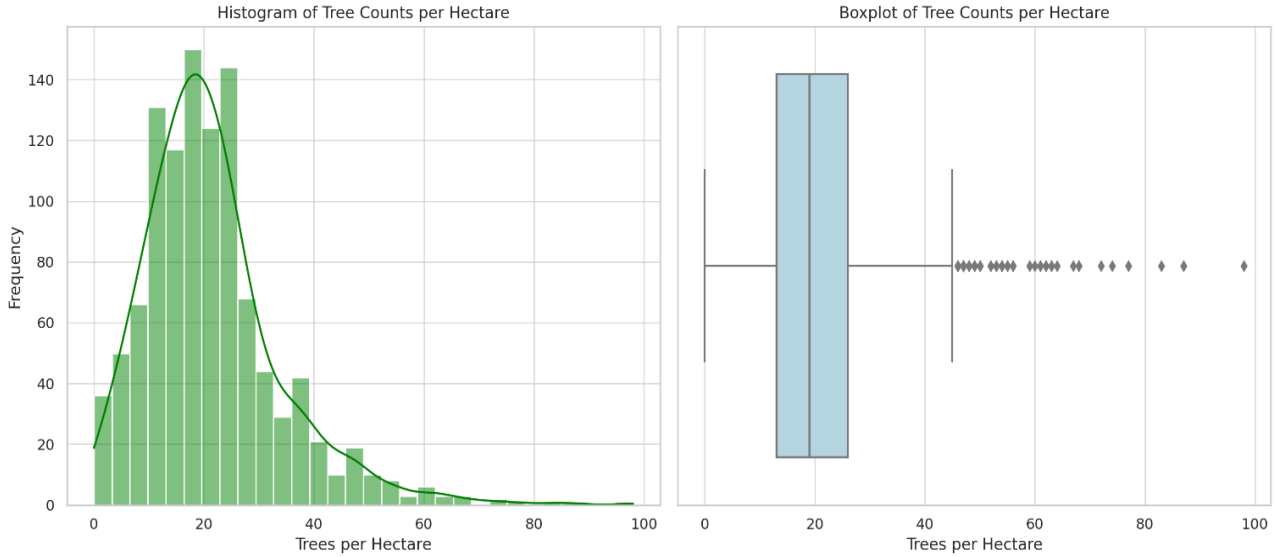

Figure 5: Histogram and Boxplot of Tree Counts per ha in the Tree-sampled Area

Table 3: Distribution of 132 Sample Plots Based on Number of Trees per Plot in Urban and Rural Landscapes

No. of Trees per Plot	No. of plots	
	Rural	Urban
3	23	15
4	18	19
5	16	16
6	7	0
7	3	3
8	2	1
Total	69	63

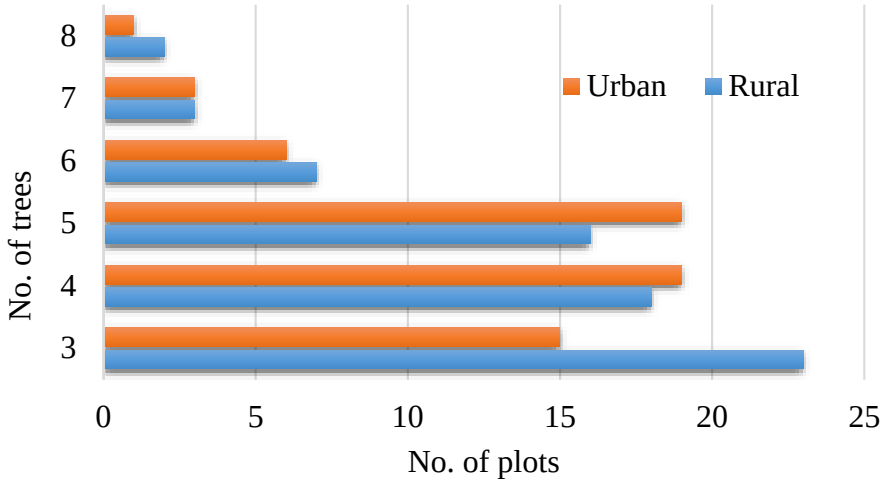

Figure 6: Heterogeneity of Tree Distribution Across Different Land Cover Type

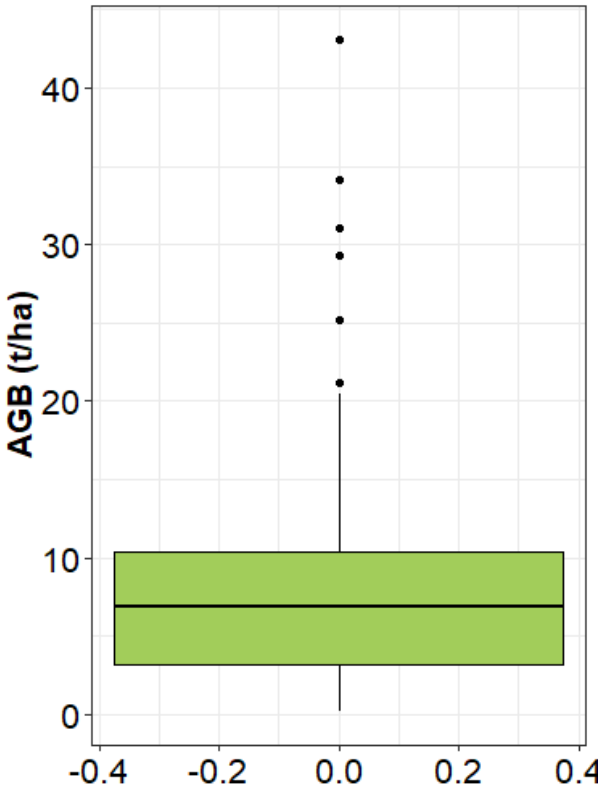

Figure 7: Boxplot Showing Field

Table 4: Statistical Summary of Field-observed AGB

AGB (t/ha)	Rural	Urban	Total
Minimum	1.06	0.19	0.19
Maximum	25.22	43.12	43.12
Mean	9.78	6.11	8.03
Median	9.16	3.46	6.88
SD	4.95	8.40	7.04

4.3 Correlation Analysis

Figure 8 illustrates the correlation matrix of remote sensing variables with field AGB. The correlation coefficients, R, ranged from -0.38 to 0.421 for all the RS variables with AGB. The overall correlation of the variables was weak to moderate, with no variable having a correlation coefficient of 0.5 or more. Further, the correlation analysis revealed that the S1 variables are highly associated with field-measured AGB compared to the S2 variables. Notably, SDI demonstrated the highest correlation coefficient (R) of 0.421, closely followed by SSRI with an R value of 0.417. With the exception of the backscattering coefficient at VH polarization (R = 0.095), all S1-derived variables exhibited a relatively stronger relationship with field AGB. In contrast, among the S2 variables, the spectral bands maintained better correlation than the VIs and BPVs.

4.4 Model Performance and Comparison for AGB Estimation

For evaluating the performance of the RS datasets individually and in combination, three models were developed and compared. To prevent the models from overfitting, highly related variables were removed through multicollinearity analysis. Among the seven parameters derived from S1, 5 were retained, generating a model (M_S1) having a moderate performance, with an R^2 value of 0.46, RMSE of 4.03 t/ha, and MAE of 3.21 t/ha. From the variable importance, the higher contribution of the SAR indices was observed (Table 5). The VH_db came as the least contributor in terms of %IncMSE and IncNodePurity. The second model (M_S2) utilized eleven variables out of the 24 from the S2 dataset. The BPVs included were LAI, CW, CAB, and FCOVER, and the VIs were EVI, DVI, GNDVI, and NDII. Further, the multispectral information from B02, B06, and B12 bands was used in M_S2. The performance of the model fell behind the M_S1, with an R^2 value of 0.43, an RMSE of 4.04 t/ha, and an MAE of 3.15 t/ha. LAI was identified as an important predictor variable in this model. LAI came as the most important predictor variable as per both %IncMSE and IncNodePurity.

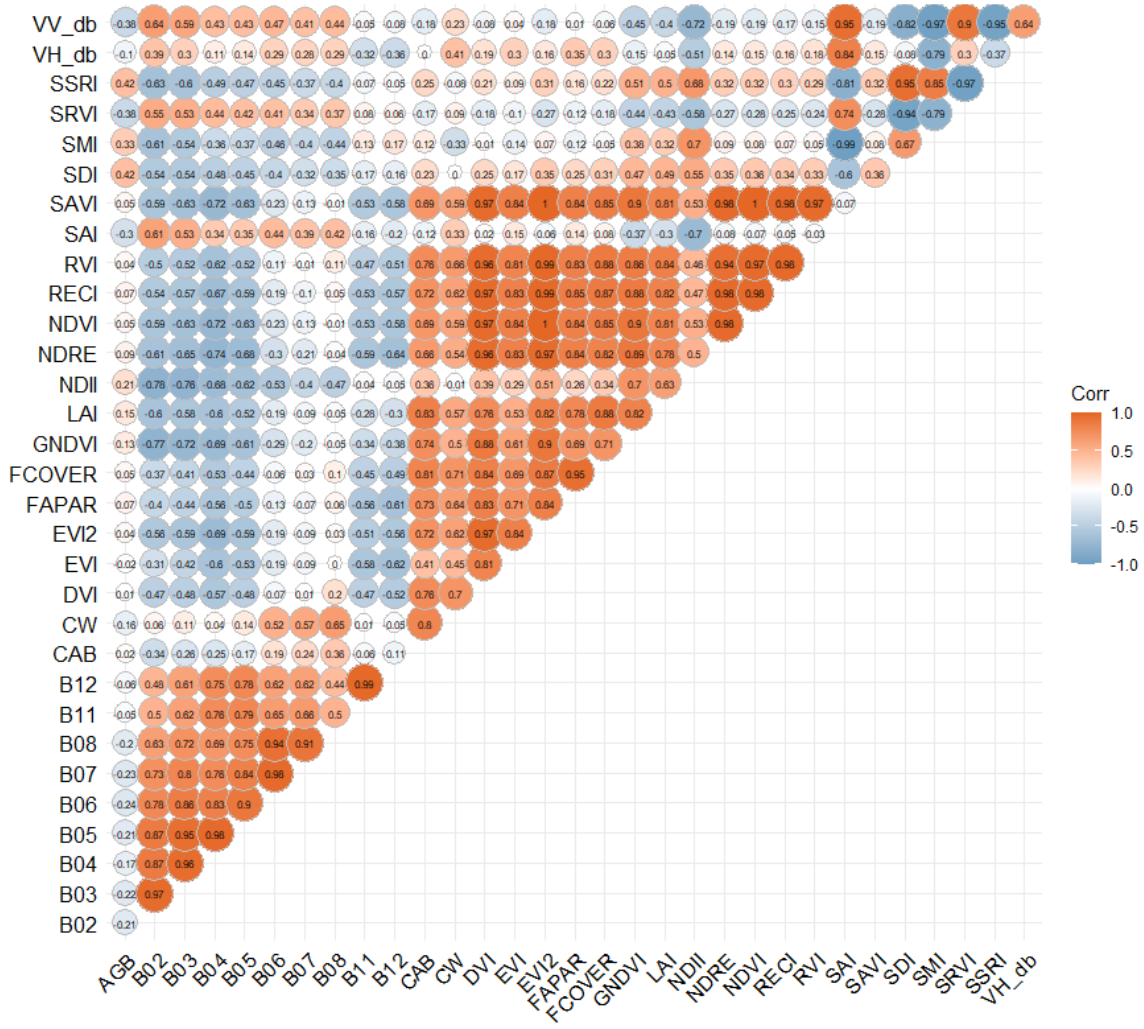

Figure 8: Correlation Matrix Between Remote Sensing Variables and Field AGB

Table 5: AGB Models Variables

Model	Predictor variables used	R^2	RMSE (t/ha)	MAE (t/ha)
M_S1	SRVI, SSRI, SDI, SAI, and VH_db	0.46	4.03	3.21
M_S2	B02, B06, B12, EVI, DVI, GNDVI, NDII, LAI, CAB, CW, and FCOVER	0.43	4.04	3.15
M_S1S2	SDI, SMI, VH_db, B02, B05, B07, B12, EVI, DVI, NDII, LAI, CW, CAB, and FCOVER	0.52	3.89	3.15

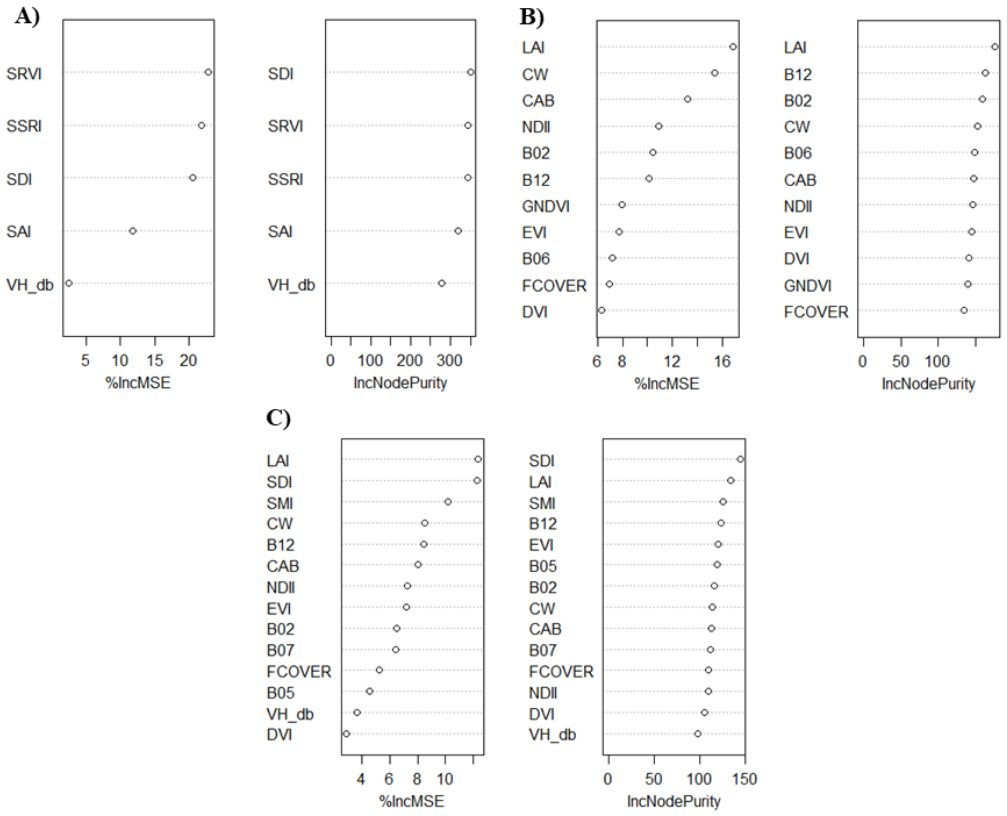

Figure 9: Variable Importance of the Models A) M_S1, B) M_S2, and C) M_S1S2

Over the above, taking a sum of 14 variables from both S1 and S2, the synergistic model, M_S1S2, gave a higher prediction accuracy as compared to the previous two models. The R^2 and RMSE values obtained for M_S1S2 were 0.52 and 3.89 t/ha, respectively. R^2 is higher than that of M_S1 and M_S2, and RMSE is found to be lower. However, MAE was found as the same as that of the multispectral data model, M_S2 (3.15 t/ha). Among the predictor variables included in M_S1S2, LAI, SDI, SMI, and B12 were among the high contributing variables to the model. Figure 9. represents the variable importance of each model. To illustrate the prediction accuracy of the developed models, scatterplots between the observed and predicted values were created and are shown in Figure 9. Though M_S1S2 gave a higher performance, the validation matrices indicated that only slight variation exists, suggesting that each model has reasonable reliability for TOF biomass estimation in arid environments. The AGB maps for all three models are given in Figure 10. Analysing the AGB maps, we noticed that M_S1 was able to predict the lowest and highest biomass values, which are 1.7 t/ha and 12.46 t/ha, respectively. Whereas, the lowest and highest AGB values predicted by M_S2 and M_S1S2 were 2.93 t/ha and 2.75 t/ha, and 9.1 t/ha and 8.98 t/ha correspondingly. In addition, we compared the predicted AGB from different models with field-observed AGB in different land cover types through a line diagram, as shown in Figure 11. The line diagram depicted the problem of overestimation in low biomass areas and underestimation of biomass in high biomass areas in all three models.

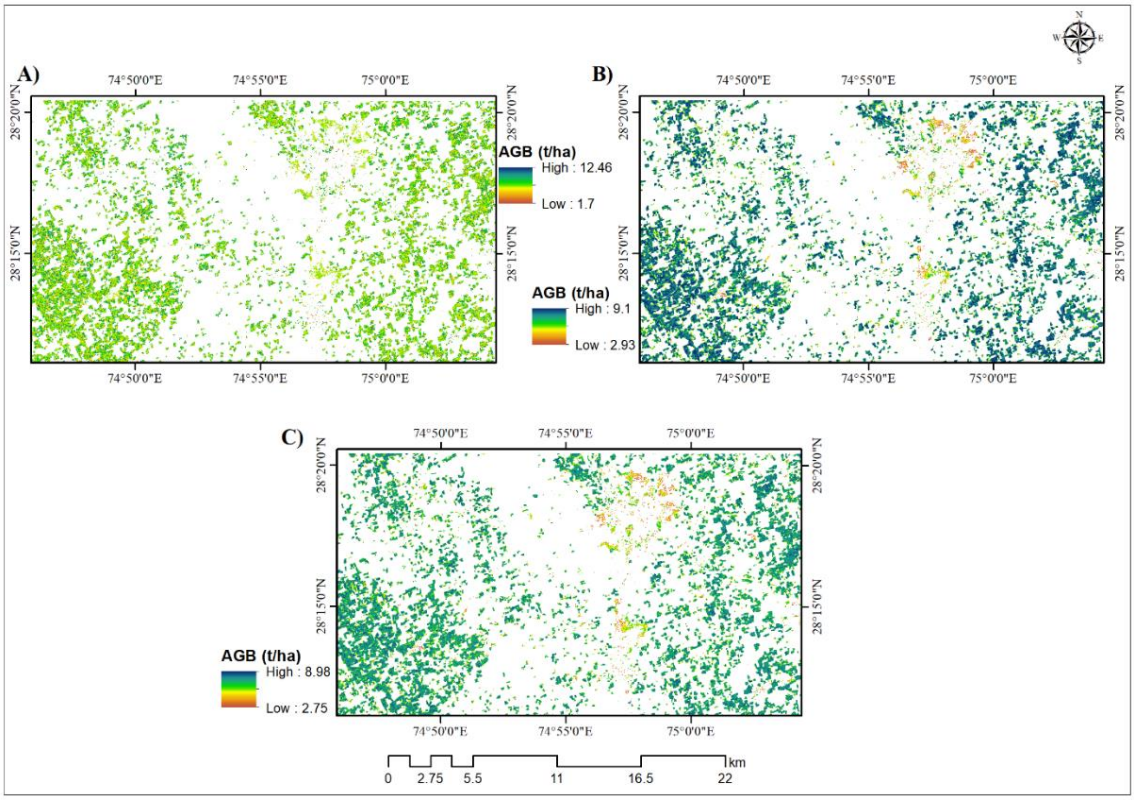

Figure 10: Spatial Distribution of AGB in the Study Area from A) M_S1, B) M_S2, and C) M_S1S2

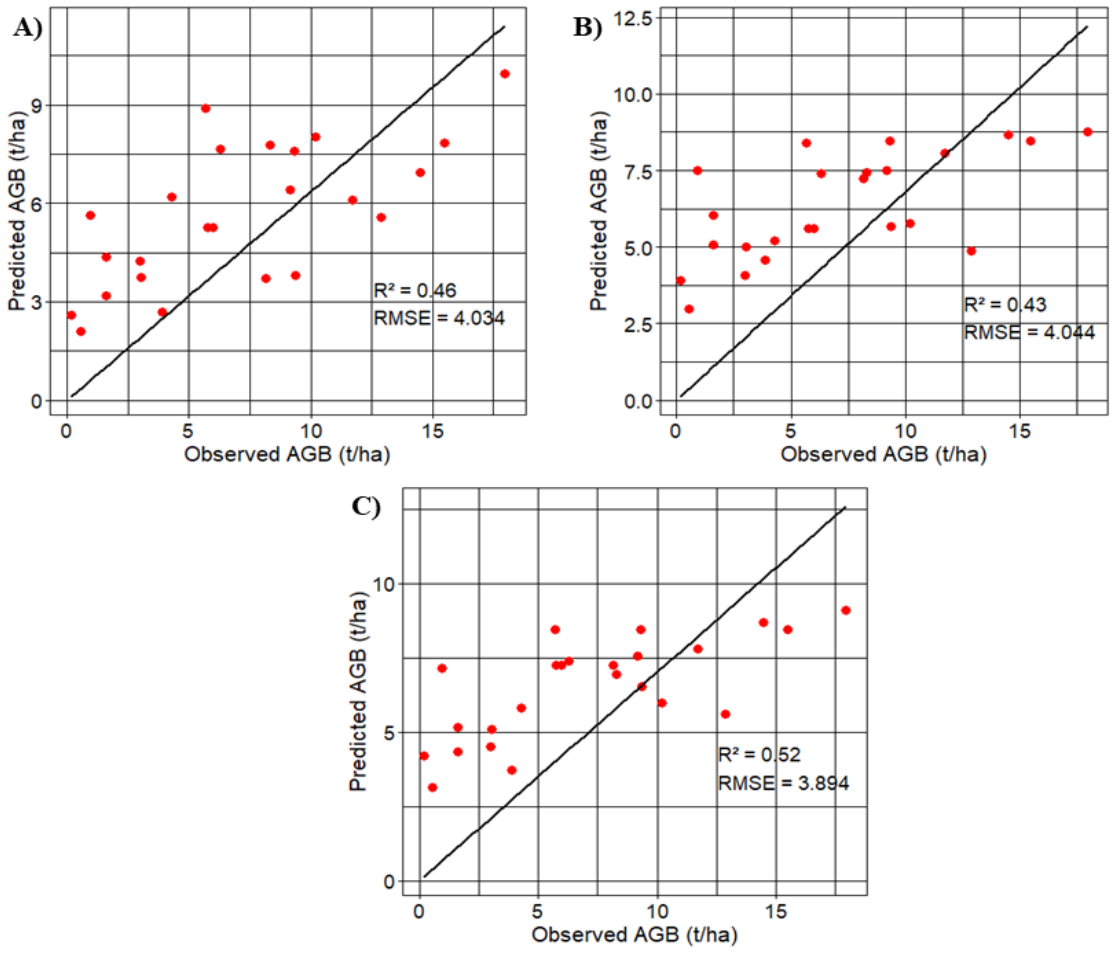

Figure 11: Scatterplot of Observed vs Predicted AGB for A) M_S1; B) M_S2; and C) M_S1S2

4.5 Discussion

Information on the biomass, carbon stock, and carbon sequestration potential of vegetation, in particular the trees outside forests, in the arid regions, highlights their importance in supporting biodiversity, rural livelihoods, and regulating the microclimate. This understanding supports the design of sustainable land management practices and enhances national greenhouse gas inventories. The highly variable vegetation density in the arid and semi-arid environments is a major constraint in biomass and carbon studies. During our study, we observed a highly discontinuous distribution of trees, with some plots having no trees at all, while others containing only isolated individuals. Since we focused on plots with a minimum of three trees, the biomass observed was notably low as compared to the dense vegetated areas. Additionally, a notable variability was noticed in the field-calculated AGB in rural and urban environments, showing the difference in land use, tree density, and species diversity (Figure 12). The number of trees in 132 plots considered varied from 3 to 8 strongly highlights the sparse vegetation, indicating the influence of other scatterers in each plot. In order to compensate the effect of non-vegetation scatterers, we incorporated different vegetation indices and biophysical variables as predictor variables as the spectral reflectance has a unique relation with the chlorophyll content in plants. The spectral reflectance has a unique relation with the chlorophyll content in plants (Lu et al. 2006).

The correlation analysis of AGB with RS variables revealed a weak to moderate relationship, where the S1 variables showed a higher relationship, indicating the enhanced sensitivity of the SAR metrics to varying biomass in the arid region. However, the backscattering coefficient at VH polarization showed a low correlation coefficient. The lower relationship of RS variables with AGB can be due to the sparse vegetation and the contribution of ground to the reflectance and the backscatter values (Anjitha et al. 2024).

In the present study, we observed that the biomass estimation models based on the RF algorithm, remote sensing datasets, and field observations gave a moderate level of predictive accuracy. Though the R^2 values obtained are not exceptionally high, it is consistent with the findings of a similar study by (Anjitha et al. 2024) conducted in semi-arid regions estimated the AGB of TOF using ALOS PALSAR-2 and S1, obtaining R^2 values ranging from 0.44 to 0.64. The sparse and heterogeneous vegetation cover is a major concern in RS-based AGB estimation. The weak signal from vegetation and background noise from the bare soil often reduce the sensitivity of both optical and SAR data to the variation in biomass.

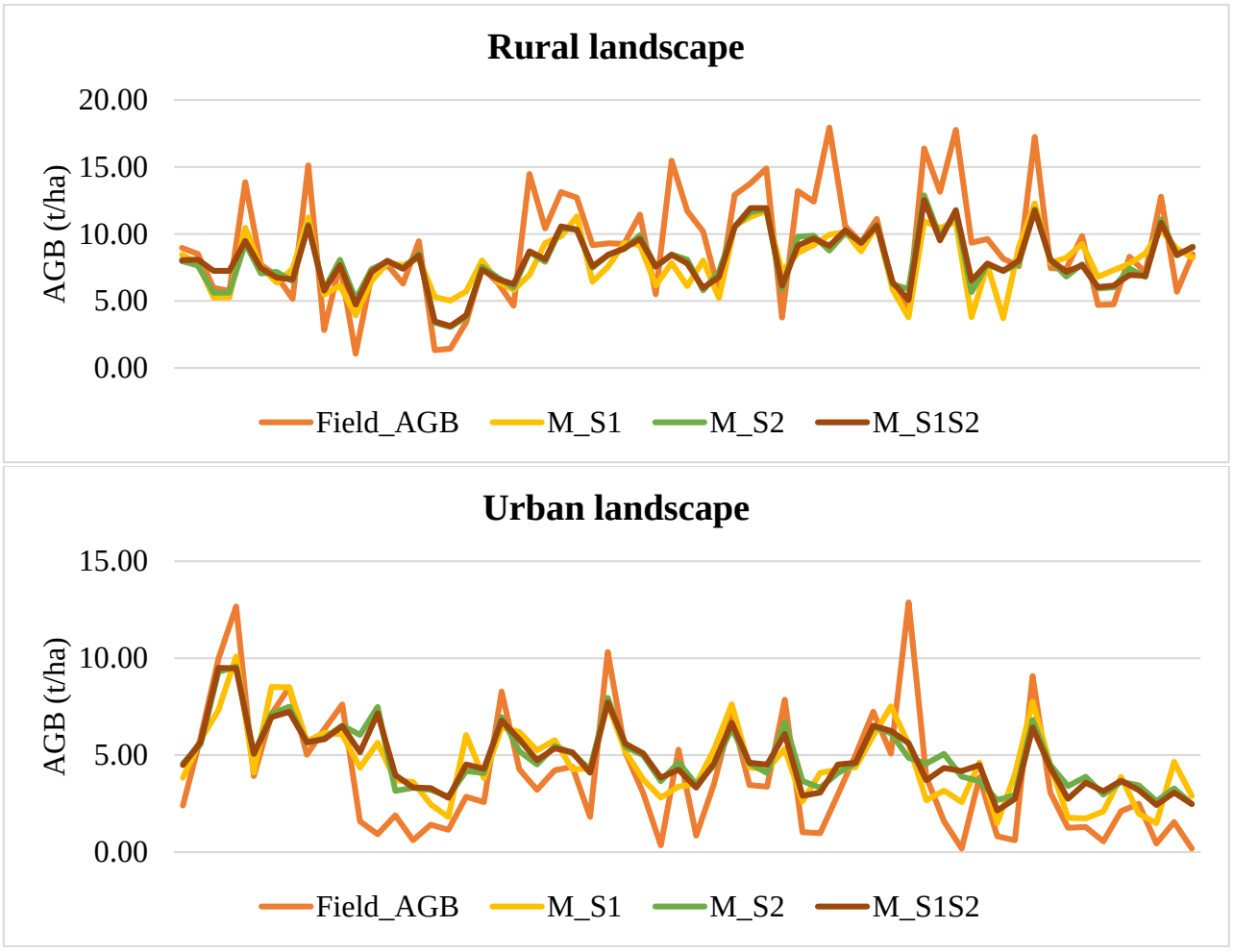

Figure 12: Line Diagram Comparing the Observed and Predicted AGB from Different Models for Different Land Cover Types

Some studies have demonstrated better performance of the S1 dataset in biomass estimation (Ndikumana et al. 2018; Crabbe et al. 2019; Bao et al. 2019), and certain studies reported the better performance of S2 (Sibanda et al. 2015; Baloloy et al. 2018; Pandit et al. 2018; Imran et al. 2020; Adamu et al. 2021). S1 backscattering coefficient at VH polarization was observed to have a high relationship with rice biomass, with the RF method yielding R^2 of 0.9 and RMSE of 162 $g.m^{-2}$ (Ndikumana et al. 2018). (Adamu et al. 2021) used the vegetation indices, such as NDVI, SAVI, DVI, and EVI2, for AGB estimation employing linear regression models in the West African Sahel Savanna and obtained moderate coefficients (R^2) between 0.43 and 0.52.

The data synergism was found to have better performance, as in our case, where we observed the S1 and S2 synergistic model (M_S1S2) had improved accuracy values as compared to the individual sensor-based models (M_S1 and M_S2), in other studies by (Navarro et al. 2019), (Chen et al. 2018), and (Nuthamachot et al. 2020). The optical dataset is capable of providing more detailed information about the surface features. On the other hand, SAR datasets with penetrative capability reveal the vertical structural information of vegetation (Sainuddin et al. 2024). Therefore, this optical and SAR data synergism holds the potential to improve biomass estimates of vegetation and is observed in previous studies as well. AGB over the temperate forest in Poland was estimated using S1 and S2 datasets and employing RF by (Agata et al. 2018). A study in the mangrove forests and their transformed land uses of the Philippines obtained high prediction values with a prediction error <29 Mg/ha (Castillo et al. 2017). Furthermore, (Chen et al. 2018) demonstrated the encouraging results obtained with S1 and S2 data synergism in the study conducted in the forests of Changbai Mountains, China, in which the backscattering coefficients and texture measures from S1 and multispectral bands, VIs, and BPVs from S2 were incorporated.

In M_S2 and M_S1S2, LAI came as one among the top contributors to the models. This aligns with the results of (Castillo et al. 2017), where they found that the AGB estimation model based on the biophysical variables from S2, LAI, was more accurate in the prediction. In addition, in M_S1 and M_S1S2 models, SAR derivatives were revealed as the most important variables than the backscattering coefficients, which is in concordance with the results obtained by (Forkuor et al. 2020). They observed that the first three important variables were the derivatives in the RF model while mapping the AGB of the Sudanian Savanna, West Africa. This lends further credibility to using the derivatives from RS data in biomass estimation studies.

Moreover, all three models showed the problem of overestimation and underestimation corresponding to low biomass and high biomass regions, respectively. This is a common problem associated with MLAs. This constraint was observed in previous studies of AGB estimation based on remote sensing technology. (Su et al. 2020) demonstrated the model saturation of RF at high and low biomass areas in the subtropical forests in Guangdong Province in China, as was the case in the Brazilian savannah (Bispo et al. 2020). (Malhi et al. 2022) observed overestimation of AGB in the RF model as compared to the linear model in their study in the tropical forests. Again, (Chen et al. 2018) noticed overestimation of all four models, GWR, ANN, SVR, and RF, in AGB prediction in the Changbai Mountains using S1 and S2 variables as the predictors. Further, overestimation in the sparsely vegetated area is often attributed to the dominant influence of the background noise from the bare soil. The strong influence of background soil drastically weakens the vegetation signal in sparse canopy environments (Ren and Zhou, 2019). Additionally, the reflectance from the mixed green and senescent herbs in arid and semi-arid regions could also have contributed to the overestimation problem. Further, the saturation limit inherent to the RS datasets is another cause of concern in the underestimation of biomass. (Okin et al. 2001) observed that the vegetation had a low spectral contrast in the arid and semi-arid environments, in contrast to the vegetation in humid environments, which can exacerbate the problem of signal saturation and reduce the detectability of biomass variations.

The findings clearly showed that the S1 and S2 datasets hold the potential for mapping AGB of scattered TOF in arid environments. Despite the modest differences in predictive accuracy, each model demonstrated reasonable reliability for biomass estimation. These results highlight the utility of medium-resolution S1 and S2 datasets for regional-scale AGB mapping in low-biomass environments, particularly where field measurements are limited. This study highlights the significance of large-scale tree inventory data in improving the accuracy and reliability in quantifying AGB.

The ecological significance of the sparse tree populations in arid regions carries substantial weight, particularly in the global carbon cycle. However, most biomass studies in India have focused on forest areas, while TOF in drylands remains underrepresented in national carbon assessments and land management strategies. The collective carbon sequestration of TOF at the landscape level and regional scales is significant, and the persistence of this woody vegetation in the water-scarce arid regions indicates the long-term storage of carbon. There is a lack of spatially explicit data for biomass in TOF in the arid regions of India. Addressing this gap is crucial for enhancing climate mitigation strategies, particularly as arid environments are more prone to land degradation and desertification.

5. Conclusions

Reliable estimates on biomass, carbon stock, and carbon sequestration potential of vegetation are significant in designing strategies for land management and climate change mitigation in the vulnerable arid environments. Employing the remote sensing technique, the above-ground biomass of trees outside forests in the arid region was estimated in this study. The potential of Sentinel-1 and Sentinel-2 datasets in isolation and in integration, applying the RF model in AGB estimation of arid regions, was analysed. Due to the scarcity and uneven distribution of the trees, the RS variables were observed to have a low to

moderate relationship with the field-observed biomass. Sentinel-1 SAR indices showed stronger correlation with field-measured AGB compared to Sentinel-2 variables. Using the predictor variables from both datasets, we developed three models, among which the synergistic model (M_S1S2) outperformed the other two models (M_S1 and M_S2), demonstrating the better performance of data synergism. However, the models showed relatively small differences in R^2 and RMSE values, providing stable estimates of AGB across the study area. The estimated AGB maps provide valuable insight into the AGB distribution of TOF, which is useful for future carbon accounting and land management planning.

Acknowledgments

We are thankful to the European Space Agency (ESA) for open access to Sentinel-1 and Sentinel-2 data. We are grateful to the Director, National Remote Sensing Centre, Hyderabad, Head, Department of Botany, Government Lohia College, and Head, Department of Environmental Sciences, All Saints' College, Thiruvananthapuram, for the facilities, support and encouragement.

References

Adam, E., O. Mutanga, and D. Rugege. 2009. "Multispectral and hyperspectral remote sensing for identification and mapping of wetland vegetation: A review." *Wetlands Ecology and Management* 18:281–296. https://doi.org/10.1007/s11273-009-9169-z.

Adamu, B., et al. 2021. "Evaluating the accuracy of spectral indices from Sentinel-2 data for estimating forest biomass in urban areas of the tropical savanna." *Remote Sensing Applications: Society and Environment* 22:100484. https://doi.org/10.1016/j.rsase.2021.100484.

Agata, H., L. Aneta, Z. Dariusz, S. Krzysztof, L. Marek, S. Christiane, and P. Carsten. 2018. "Forest aboveground biomass estimation using a combination of Sentinel-1 and Sentinel-2 data." Pp. 9026–9029 in *IGARSS 2018—2018 IEEE International Geoscience and Remote Sensing Symposium*. IEEE. https://doi.org/10.1109/igarss.2018.8517965.

Anand, A., P. C. Pandey, G. P. Petropoulos, A. Pavlides, P. K. Srivastava, J. K. Sharma, and R. K. Malhi. 2020. "Use of Hyperion for mangrove forest carbon stock assessment in Bhitarkanika Forest Reserve: A contribution towards blue carbon initiative." *Remote Sensing* 12:597. https://doi.org/10.3390/rs12040597.

Anjitha, A. S., C. S. Reddy, N. N. Sri Surya, K. V. Satish, and S. V. Asok. 2024. "Estimating above-ground biomass of trees outside forests using multi-frequency SAR data in the semi-arid regional landscape of southern India." *Spatial Information Research* 32:593–605. https://doi.org/10.1007/s41324-024-00582-0.

Baloloy, A. B., et al. 2018. "Estimation of mangrove forest aboveground biomass using multispectral bands, vegetation indices and biophysical variables derived from optical satellite imageries." *ISPRS Annals of the Photogrammetry, Remote Sensing and Spatial Information Sciences* IV–3:29–36. https://doi.org/10.5194/isprs-annals-iv-3-29-2018.

Bao, N., W. Li, X. Gu, and Y. Liu. 2019. "Biomass estimation for semiarid vegetation and mine rehabilitation using WorldView-3 and Sentinel-1 SAR imagery." *Remote Sensing* 11:2855. https://doi.org/10.3390/rs11232855.

Bestelmeyer, B. T., G. S. Okin, M. C. Duniway, S. R. Archer, N. F. Sayre, J. C. Williamson, and J. E. Herrick. 2015. "Desertification, land use, and the transformation of global drylands." *Frontiers in Ecology and the Environment* 13(1):28–36.

Bispo, P. D. C., et al. 2020. "Woody aboveground biomass mapping of the Brazilian savanna with a multi-sensor and machine learning approach." *Remote Sensing* 12(17):2685. https://doi.org/10.3390/rs12172685.

Bordoloi, R., et al. 2022. "Satellite-based integrated approaches to modelling spatial carbon stock and carbon sequestration potential of different land uses of Northeast India." *Environmental and Sustainability Indicators* 13:100166. https://doi.org/10.1016/j.indic.2021.100166.

Breiman, Leo. 2001. "Random forests." *Machine Learning* 45:5–32. https://doi.org/10.1023/A:1010933404324.

Carreiras, J. M., M. J. Vasconcelos, and R. M. Lucas. 2012. "Understanding the relationship between aboveground biomass and ALOS PALSAR data in the forests of Guinea-Bissau." *Remote Sensing of Environment* 121:426–442. https://doi.org/10.1016/j.rse.2012.02.012.

Cartus, O., M. Santoro, U. Wegmuller, N. Labriere, and J. Chave. 2022. "Sentinel-1 coherence for mapping above-ground biomass in semiarid forest areas." *IEEE Geoscience and Remote Sensing Letters* 19:1–5. https://doi.org/10.1109/lgrs.2021.3071949.

Castillo, J. A., A. A. Apan, T. N. Maraseni, and S. G. Salmo. 2017. "Estimation and mapping of above-ground biomass of mangrove forests using Sentinel imagery." *ISPRS Journal of Photogrammetry and Remote Sensing* 134:70–85. https://doi.org/10.1016/j.isprsjprs.2017.10.016.

Chang, J., and M. Shoshany. 2016. "Mediterranean shrublands biomass estimation using Sentinel-1 and Sentinel-2." Pp. 5300–5303 in *IGARSS 2016 IEEE International Geoscience and Remote Sensing Symposium*. IEEE. https://doi.org/10.1109/igarss.2016.7730380.

Chave, J., et al. 2014. "Improved allometric models to estimate the aboveground biomass of tropical trees." *Global Change Biology* 20(10):3177–3190.

Chen, L., C. Ren, B. Zhang, Z. Wang, and Y. Xi. 2018. "Estimation of forest above-ground biomass using geographically weighted regression and machine learning." *Forests* 9:582. https://doi.org/10.3390/f9100582.

Cheng, T., R. Song, D. Li, K. Zhou, H. Zheng, X. Yao, et al. 2017. "Spectroscopic estimation of biomass in canopy components of paddy rice." *Remote Sensing* 9(4):319.

Crabbe, R. A., D. W. Lamb, C. Edwards, K. Andersson, and D. Schneider. 2019. "Potential of Sentinel-1 radar to estimate pasture biomass." *Remote Sensing* 11:872. https://doi.org/10.3390/rs11070872.

David, R. M., N. J. Rosser, and D. N. Donoghue. 2022. "Improving above-ground biomass estimates of Southern Africa dryland forests." *Remote Sensing of Environment* 282:113232. https://doi.org/10.1016/j.rse.2022.113232.

dos Santos, J. R., L. S. de Araujo, T. M. Kuplich, C. da Costa Freitas, L. V. Dutra, S. J. S. Sant'Anna, and F. F. Gama. 2009. "Tropical forest biomass and its relationship with P-band SAR data." *Revista Brasileira de Cartografia* 1:58.

ESA. 2020. *WorldCover 2020*. Retrieved October 17, 2025 (https://worldcover2020.esa.int/).

FAO. 2005. *Trees outside forests*. Rome: Food and Agriculture Organization of the United Nations.

Filipponi, F. 2019. "Sentinel-1 GRD preprocessing workflow." P. 11 in *Proceedings of the 3rd International Electronic Conference on Remote Sensing*. MDPI. https://doi.org/10.3390/ecrs-3-06201.

Forkuor, G., et al. 2020. "Above-ground biomass mapping in West African dryland forest." *Remote Sensing of Environment* 236:111496. https://doi.org/10.1016/j.rse.2019.111496.

Gitelson, A. A., Y. J. Kaufman, and M. N. Merzlyak. 1996. "Use of a green channel in remote sensing of vegetation." *Remote Sensing of Environment* 58(3):289–298.

Gitelson, A. A., A. Viña, V. Ciganda, D. C. Rundquist, and T. J. Arkebauer. 2005. "Remote estimation of canopy chlorophyll content." *Geophysical Research Letters* 32.

Gitelson, A., and M. N. Merzlyak. 1994. "Quantitative estimation of chlorophyll-a using reflectance spectra." *Journal of Photochemistry and Photobiology B* 22:247–252.

Google. n.d. *Google Earth Pro*. Retrieved February 6, 2025 (https://www.google.com/earth/).

Haughton, N., G. Abramowitz, M. G. De Kauwe, and A. J. Pitman. 2018. "Does predictability of fluxes vary between FLUXNET sites?" *Biogeosciences* 15(14):4495–4513.

Hu, T., et al. 2016. "Mapping global forest aboveground biomass with LiDAR and optical imagery." *Remote Sensing* 8:565.

Huete, A. R. 1988. "A soil-adjusted vegetation index (SAVI)." *Remote Sensing of Environment* 25:295–309.

Hunt, E. R., and B. N. Rock. 1989. "Detection of changes in leaf water content." *Remote Sensing of Environment* 30:43–54.

Issa, S., B. Dahy, T. Ksiksi, and N. Saleous. 2020. "A review of terrestrial carbon assessment methods." *Remote Sensing* 12(12):2008.

Jiang, Z., A. Huete, K. Didan, and T. Miura. 2008. "Development of a two-band enhanced vegetation index." *Remote Sensing of Environment* 112:3833–3845.

Jordan, C. F. 1969. "Derivation of leaf-area index from quality of light." *Ecology* 50:663–666.

Kar, A., P. C. Moharana, and P. Raina. 2009. "Desertification and its control in major arid regions." *Journal of Earth System Science* 118(5):599–603.

Kumar, L., and O. Mutanga. 2017. "Remote sensing of above-ground biomass." *Remote Sensing* 9:935.

Kumar, S., R. D. Garg, H. Govil, and S. P. S. Kushwaha. 2019. "PolSAR-based modeling for biomass estimation." *Remote Sensing* 11:2287.

Kumar, S., U. Pandey, S. P. S. Kushwaha, R. S. Chatterjee, and W. Bijker. 2012. "Aboveground biomass estimation using Envisat SAR data." *Journal of Applied Remote Sensing* 6:063588.

Lee, J. S., L. Jurkevich, P. Dewaele, P. Wambacq, and A. Oosterlinck. 1994. "Speckle filtering of SAR images: A review." *Remote Sensing Reviews* 8(4):313–340.

Liu, H. Q., and A. Huete. 1995. "A feedback-based modification of NDVI." *IEEE Transactions on Geoscience and Remote Sensing* 33:457–465.

Lu, D. 2006. "The potential and challenge of remote sensing-based biomass estimation." *International Journal of Remote Sensing* 27(7):1297–1328.

Malhi, R. K., et al. 2022. "Synergistic evaluation of Sentinel-1 and Sentinel-2 for biomass estimation." *Advances in Space Research* 69:1752–1767.

Mertia, R. S., R. Prasad, and P. Narain. 2010. "Soil properties of degraded lands in Thar Desert." *Annals of Arid Zone* 49(2):137–144.

Nasirzadehdizaji, R., et al. 2019. "Sensitivity analysis of Sentinel-1 SAR parameters." *Applied Sciences* 9(4):655.

Navarro, J. A., et al. 2019. "Integration of UAV and Sentinel data for biomass monitoring." *Remote Sensing* 11:77.

Ndikumana, E., D. Ho Tong Minh, H. T. Dang Nguyen, N. Baghdadi, D. Courault, L. Hossard, and I. El Moussawi. 2018. "Estimation of rice height and biomass using SAR Sentinel-1." *Remote Sensing* 10:1394.

Okin, G. S., D. A. Roberts, B. Murray, and W. J. Okin. 2001. "Limits on hyperspectral vegetation discrimination." *Remote Sensing of Environment* 77(2):212–225.

Pandey, P. C., A. Anand, and P. K. Srivastava. 2019. "Mangrove species distribution and biomass assessment." *Biodiversity and Conservation* 28:2143–2162.

Pandit, S., S. Tsuyuki, and T. Dube. 2018. "Estimating above-ground biomass using Sentinel-2." *Remote Sensing* 10:601.

Rapiya, M., A. Ramoelo, and W. Truter. 2023. "Seasonal evaluation of aboveground biomass in rangelands." *Environmental Monitoring and Assessment* 195.

Rathore, V. S., N. S. Nathawat, S. Bhardwaj, and B. M. Yadav. 2018. "Prosopis juliflora invasion in Thar Desert." *Journal of Arid Environments* 153:21–28.

Reddy, C. S., K. Athira, and S. Mudalkar. 2025. "Evolution of global biodiversity monitoring." *Journal of the Indian Society of Remote Sensing*.

Reddy, C. S., C. S. Jha, P. G. Diwakar, and V. K. Dadhwal. 2015. "Nationwide classification of forest types of India." *Environmental Monitoring and Assessment* 187(12):777.

Ren, H., and G. Zhou. 2019. "Estimating green biomass ratio in arid grasslands." *Ecological Indicators* 98:568–574.

Rouse, J., R. H. Haas, J. A. Schell, and D. W. Deering. 1974. "Monitoring vegetation systems in the Great Plains." *NASA Special Publication* 351:309.

Sainuddin, F. V., S. Chirakkal, S. V. Asok, A. K. Das, and D. Putrevu. 2023. "Evaluation of multifrequency SAR data for biomass estimation." *Environmental Monitoring and Assessment* 195.

Sainuddin, F. V., G. Malek, A. Rajwadi, P. S. Nagar, S. V. Asok, and C. S. Reddy. 2024. "Estimating above-ground biomass using machine learning and multisensor data." *Journal of the Indian Society of Remote Sensing* 52:885–902.

Schnell, S., D. Altrell, G. Ståhl, and C. Kleinn. 2014. "Contribution of trees outside forests to biomass and carbon stocks." *Environmental Monitoring and Assessment* 187.

Sibanda, M., O. Mutanga, and M. Rouget. 2015. "Sentinel-2 spectral resolution in biomass estimation." *ISPRS Journal of Photogrammetry and Remote Sensing* 110:55–65.

Singh, K., and P. Chand. 2012. "Tree outside forest phytomass and carbon estimation." *Journal of Earth System Science* 121:1469–1482.

Small, D., and A. Schubert. 2008. *Guide to ASAR geocoding*. ESA-ESRIN Technical Note.

Srivastava, P. K., R. K. Malhi, P. C. Pandey, A. Anand, P. Singh, M. K. Pandey, and A. Gupta. 2020. "Revisiting hyperspectral remote sensing." Pp. 3–21 in *Hyperspectral Remote Sensing*. Elsevier.

Su, H., W. Shen, J. Wang, A. Ali, and M. Li. 2020. "Machine learning and geostatistical approaches for biomass estimation." *Forest Ecosystems* 7:64.

Sulabha, A. A., S. V. Asok, C. S. Reddy, and K. Soumya. 2025. "Aboveground biomass estimation in tropical forests: A systematic review." *Journal of the Indian Society of Remote Sensing* 53:653–679.

Sun, X., G. Li, M. Wang, and Z. Fan. 2019. "Uncertainty in estimating forest aboveground biomass." *Remote Sensing* 11:722.

Torabzadeh, H., M. Moradi, and P. Fatehi. 2019. "Estimating aboveground biomass in Zagros forest." *ISPRS Archives* XLII-4/W18:1059–1063.

Van Pham, M., et al. 2019. "Integrating Sentinel-1A SAR data and GIS for biomass estimation." *Remote Sensing Applications: Society and Environment* 14:148–157.

Zandler, H., A. Brenning, and C. Samimi. 2015. "Quantifying dwarf shrub biomass in arid environments." *Remote Sensing of Environment* 158:140–155.